HYDROLOGICAL PROCESSES
Hydrol. Process. **21**, 2610–2622 (2007)
Published online in Wiley InterScience
(www.interscience.wiley.com) DOI: 10.1002/hyp.6792

A simple heat-conduction method for simulating the frost-table depth in hydrological models

Masaki Hayashi,[1]* Neil Goeller,[2] William L. Quinton[3] and Nicole Wright[4]

[1] *Department of Geology and Geophysics, University of Calgary, Calgary, Alberta, Canada*
[2] *Golder Associates, Victoria, British Columbia, Canada*
[3] *Cold Regions Research Centre, Wilfrid Laurier University, Waterloo, Ontario, Canada*
[4] *Department of Geography, Simon Fraser University, Burnaby, British Columbia, Canada*

Abstract:

Hillslope runoff in permafrost regions covered by organic soil is strongly influenced by subsurface flow in the active layer, as well as surface flow where the active layer is very shallow. Flow rates in the organic-rich active layer are strongly dependent on the depth to the thawing front (i.e. frost table) and the corresponding soil hydraulic conductivity at that depth. Therefore, hydrological models for permafrost terrains need to simulate the thawing of the active layer accurately. In order to simulate the downward movement of the frost table, a simple heat-conduction model was proposed and compared to field data from a wet, organic-covered watershed in a discontinuous permafrost region of Canada. Ground heat flux was measured simultaneously using the calorimetric, gradient, and flux-plate methods to increase the confidence in data sets. The majority (>86%) of ground heat flux was used to melt the ice in frozen soil, and the soil temperature had a linear profile from the ground surface to the frost table when averaged over several days. Assuming a linear temperature profile, the proposed method calculates the daily rate of thawing from ground surface temperature and bulk thermal conductivity, where the latter is essentially determined by soil water content. Simulated depths to the frost table during three thaw seasons (2003–2005) matched closely with the observed data for two contrasting ground-cover types with distinctly different thaw rates. The method can be easily implemented in hydrological models, and will provide a useful tool for simulating hillslope drainage in organic-covered permafrost terrains, and for evaluating the effects of topography and land cover on the temporal and seasonal variability of the frost table. Copyright © 2007 John Wiley & Sons, Ltd.

KEY WORDS permafrost; frozen ground; active layer; thermal conductivity; peat; organic soil

Received 1 June 2006; Accepted 11 December 2006

INTRODUCTION

Permafrost plays an important role in the northern hydrological cycle (Woo and Winter, 1993). Organic soils dominate much of the permafrost regions of North America, including tundra, taiga and wetlands (SCWG, 1998), and are composed of partially to well decomposed plant remains that have accumulated since de-glaciation. Runoff processes in organic-covered permafrost terrains are distinct in that the dominant runoff mechanism is subsurface flow through the seasonally thawed organic layer (Quinton and Marsh, 1999). Seasonal ice in the active layer limits lateral subsurface drainage to the saturated zone perched above the frozen-saturated soil. As soil thawing progresses, the frost table and the thawed saturated zone above it descend through the soil profile (Woo, 1986; Metcalfe and Buttle, 1999), while the saturated hydraulic conductivity of peat decreases by orders of magnitude with depth (Chason and Siegel, 1986; Quinton *et al*., 2000; Beckwith *et al*., 2003). Therefore, the rate of subsurface flow in organic-covered permafrost terrains is strongly influenced by the depth to the frost table and the corresponding soil hydraulic conductivity at that depth (Quinton and Gray, 2001). In order to represent subsurface flows properly, hydrological models for permafrost terrains need to simulate the thawing of the active layer accurately (Zhang *et al*., 2000).

The energy for thawing frozen soil is transferred from the ground surface to the frost table primarily by thermal conduction, although non-conductive processes such as infiltration may contribute appreciably in some cases (Kane *et al*., 2001). Noting that the rate of thermal conduction is strongly dependent on the temperature gradient between the ground surface and the frost table, temperature index methods derived from the Stefan equation have been used by many researchers to predict the thickness of the active layer (Nelson and Outcalt, 1987) or seasonal progression of the frost table (Nelson *et al*., 1997). The Stefan equation in the permafrost literature takes the form of (Jumikis, 1977, p. 205):

$$z = [(2n\lambda_b t T_{av})/(\rho f L)]^{1/2} \quad (1)$$

where z (m) is the depth to the frost table, λ_b (W m^{-1} °C^{-1}) is the bulk thermal conductivity of thawed soil, t (s) is the elapsed time since the beginning of thawing, T_{av} (°C) is mean air temperature between time zero and t, ρ (kg m^{-3}) is the density of ice, f is the

* Correspondence to: Masaki Hayashi, Department of Geology and Geophysics, University of Calgary, Calgary, Alberta, T2N 1N4, Canada. E-mail: hayashi@ucalgary.ca

volumetric fraction of ice in frozen soil, and L (J kg^{-1}) is the latent heat of fusion. The n-factor in Equation (1) is the ratio of ground-surface to air temperature (Klene *et al*., 2001), which relates mean air temperature to mean surface temperature that controls thermal conduction. The soil parameters and n in Equation (1) have large spatial and temporal variability, and hence, temperature-index methods are commonly expressed as:

$$z = \beta\, DDT^{1/2} \tag{2}$$

where β (m d$^{-1/2}$ °C$^{-1/2}$) is an empirical factor determined by regression and DDT (d °C) is the degree-day sum of air temperature over the thawing period (Hinkel and Nicholas, 1995). While Equation (2) provides a useful tool for assessing the spatial variability of active-layer thickness and its sensitivity to climate variability (Nelson *et al*., 1997; Anisimov *et al*., 2002; Shur *et al*., 2005), its use in hydrological models is limited by the transferability of the empirical factor.

Instead of taking empirical approaches such as Equation (2), one can numerically solve coupled heat and mass transfer equations to simulate the thawing process if detailed information on soil properties and boundary conditions are available (e.g. Zhao *et al*., 1997; Romanovsky and Osterkamp, 2000; Roth and Boike, 2001). However, numerical solution of the non-linear, coupled equations is computationally intensive, which makes it impractical to use in large-scale hydrological models. A relatively simple numerical algorithm is needed to model the thawing of the organic layer that strikes a balance between computational efficiency and faithful representation of physical processes.

Equation (1) indicates that the variability of thawing depths is due to the variability of soil thermal conductivity and volumetric ice fraction, as well as atmospheric forcing. Therefore, the thawing algorithm in hydrological models needs to represent these factors in a simple but physically based manner. Noting that land-surface schemes (e.g. Verseghy *et al*., 1993) used in hydrological models compute ground-surface temperature as a state variable, it is desirable to use surface temperature to provide the atmospheric forcing, instead of using air temperature multiplied by the n-factor (Equation (1)). The thermal conductivity of peat is essentially determined by its water content because peat generally has high porosity (>0·70), and the organic material itself has a relatively low thermal conductivity compared to mineral soil. Therefore, thermal conductivity can be estimated reasonably well from water content, which is a state variable in most hydrological models (e.g. Cherkauer and Lettenmaier, 1999) along with volumetric ice fraction. For these reasons, a simple thawing algorithm using ground-surface temperature as the forcing variable and thermal conductivity as a function of water content is a promising alternative to the empirical Equation (2). The objective of this paper is to: (1) describe a simple heat-conduction method for simulating the depth to the frost table in organic-covered permafrost regions during soil thawing; (2) evaluate the performance of the new method using detailed field data; and (3) examine the inter-site transferability of the method.

METHODS

Heat conduction equation

In organic-covered, permafrost regions, the majority of the ground heat flux is consumed by the latent energy required to melt ice in the active layer, and thereby lower the frost table (Roulet and Woo, 1986; Halliwell and Rouse, 1987). Therefore, the rate of frost-table lowering can be approximated by a simple conduction equation:

$$\rho f L \frac{dz}{dt} = \lambda_b \frac{T_s - 0}{z} \tag{3}$$

where T_s (°C) is ground-surface temperature and 0 (°C) is the temperature at the frost table. It is assumed that: (1) the energy used to warm the thawed layer above the frost table and conduction to the frozen peat below the frost table is relatively small; and (2) the temperature distribution within the thawed layer is linear. Validity of the two assumptions will be examined below using field data. It should be noted that Equation (3) assumes that T_s remains at or above 0 °C and, hence, cannot be used in cases where prolonged periods of sub-zero T_s occur during a thawing season. Equation (3) can be incorporated into hydrological models to calculate the daily position of the frost table. An integrated form of Equation (3) (see Appendix for derivation) will be used to evaluate this method:

$$z = \alpha(86\,400 \Sigma \lambda_b T_s)^{1/2} \tag{4}$$

where $\Sigma\lambda_b T_s$ is the cumulative sum of the product of daily average λ_b and T_s, and α (J$^{-1/2}$ m$^{3/2}$) is a constant defined by:

$$\alpha = [2/(\rho f L)]^{1/2} \tag{5}$$

Equation (4) is a modified form of the Stefan equation (Equation (1)).

Field site

Field data were collected at the Scotty Creek watershed (61°18′N; 121°18′W) in a wetland-dominated, discontinuous permafrost zone of the Northwest Territories, Canada (Figure 1(a)). The nearest climate station is in Fort Simpson, located 50 km to the north. Mean annual air temperature and precipitation in Fort Simpson are −3·2 °C and 369 mm, respectively, with 46% of annual precipitation falling as snow (MSC, 2002). Snowmelt usually begins in late March and continues through most of April, with small amounts of snow remaining into May. The stratigraphy in this region includes an organic layer of varying thickness (*ca.* 0·5–8 m) overlying a silt-sand layer, below which lies a thick-clay to silt-clay deposit (Aylesworth and Kettles, 2000). Dominant landscapes within the watershed are peat plateau, channel fen,

DOI: 10.1002/hyp

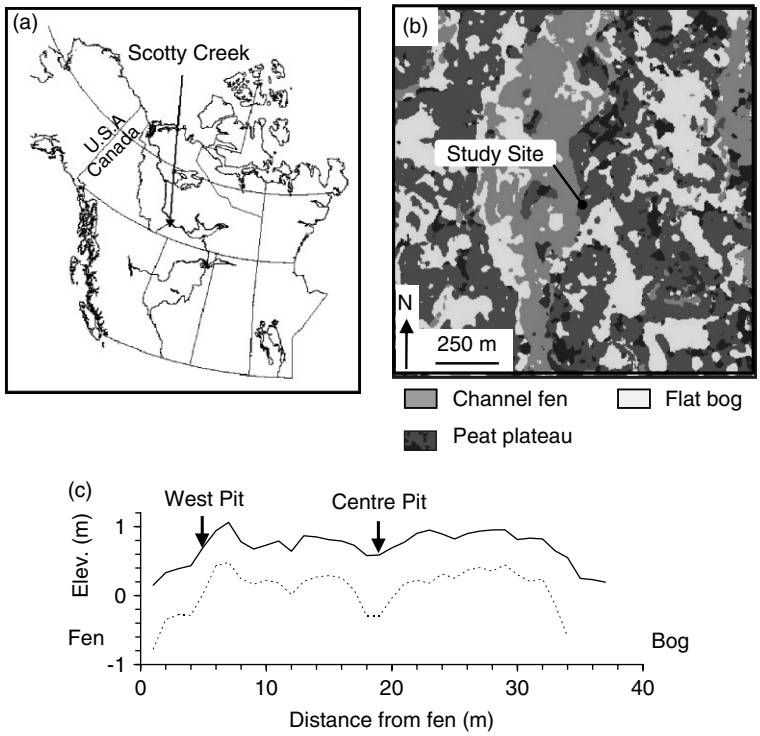

Figure 1. (a) Location of Scotty Creek. (b) Map around the study site showing three major land-cover types classified on an IKONOS satellite image acquired on 13 September 2000 (Hayashi *et al*., 2004). (c) West-east cross section of the study site starting from the channel fen. The solid line indicates the ground surface elevation with respect to the fen water surface, and the dashed line indicates the frost table measured on 5 September 2005

and flat bog (Figure 1(b)) (Quinton *et al*., 2003). Only the peat plateaus overlie permafrost, while bogs and fens experience seasonal freeze-thaw (Robinson and Moore, 1999). The permafrost thickness has not been measured in the study site, but Burgess and Smith (2000) reported 5–10 m in the boreholes under peat-covered sites near Fort Simpson.

Instrumented sites were established in August 2001 on a peat plateau (Figure 1(b)), and gradually expanded with additional sensors during 2002–2005. The ground surface of the peat plateau rises about 1 m above the adjacent bogs and fens (Figure 1(c)). Relatively short (<5–10 m) black spruce (*Picea mariana*) trees grow sparsely on the plateau, and the ground cover is composed of lichens and mosses overlying sylvic peat containing dark, woody material and the remains of lichen, rootlets and needles. The ground surface is relatively dry, and the flow of subsurface water is normally restricted to the thawed, saturated zone between the water table and the frost table (Hayashi *et al*., 2004).

The soil has a two-layer structure, where the top 0·1–0·15 m consists of living plants and relatively undecomposed organic material overlying peat in a more advanced state of decomposition. This structure is reflected in the profile of dry bulk density and porosity (Figure 2), which were measured on samples collected from 12 soil pits using standard soil sample tins, 5·4 cm in diameter (sample volume = 92 cm^3). It is determined that the top 0·15 m has an average porosity of 0·92 for 19 samples, and the layer below has an average porosity of 0·82 for 24 samples.

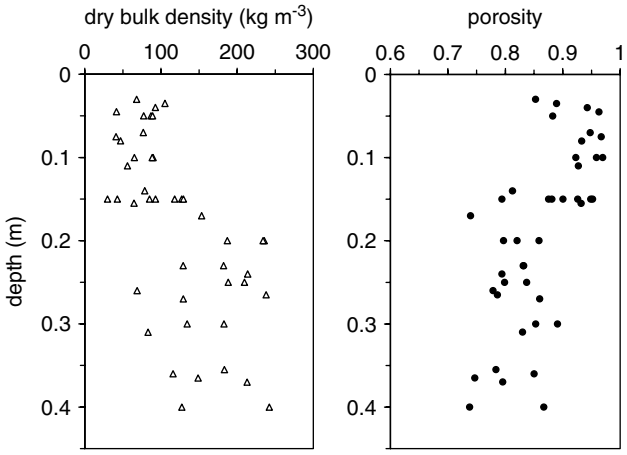

Figure 2. Dry bulk density and porosity of peat samples collected at the Scotty Creek site

Site instrumentation

Two soil pits, separated by 14 m, were excavated upto the frost table on 20 August 2001, for the purpose of installing soil sensors. Approximate locations of the two pits are shown in Figure 1(c), although Centre and West Pits were located approximately 2·5 and 1 m, respectively, away from the survey line. The groundcover of Centre Pit was approximately half-half mixture of moss and lichen, while West Pit was predominantly lichen-covered. The depth to the frost table was 0·7 m in the Centre Pit and 0·5 m in West Pit at the time of installation (August 20). Thermistor probes (Campbell Scientific, 107) were installed at depths of 0·05, 0·1, 0·15,

DOI: 10.1002/hyp

0·2, 0·25, 0·3, 0·4, 0·5, 0·6, and 0·7 m in Centre Pit and 0·5, 0·1, 0·2, 0·3, and 0·5 m in West Pit. Water content reflectometers (WCR) (Campbell Scientific, CS615) were installed at depths of 0·1, 0·2, 0·3, and 0·4 m in Centre Pit and 0·2 m in West Pit; and calibrated against the water content of peat samples collected at the time of installation (Quinton *et al*., 2005). A heat flux plate (Campbell Scientific, HFT3) was installed at a depth of 0·05 m in Centre Pit and calibrated as described below. Following the installation of sensors, the pits were backfilled with the excavated material, preserving the original layering and groundcover as much as possible.

Air temperature was measured near Centre Pit in 2003 and at a meteorological station located between the two pits in 2004 and 2005 using a thermistor housed in a Gill radiation shield. Net radiation was measured at the meteorological station using a four-component radiometer (Kipp & Zonen, CNR1) in 2004 and 2005, located 2 m above a moss-covered ground surface. Ground-surface temperature was measured using an infrared thermocouple (IRT) sensor (Apogee Instruments, IRTS-P) located 1·5 m above Centre Pit. Snow depth was measured manually using a ruler at Centre Pit, and rainfall was measured using a tipping-bucket rain gauge (Jarek Manufacturing) located at the meteorological station. All sensors were connected to dataloggers (Campbell Scientific, CR10X), programmed to measure every minute and record hourly or half-hourly averaged values.

Instrumental accuracy of the IRT sensor was 0·3 °C according to the manufacturer's specification. In order to evaluate the accuracy of the IRT sensor further, surface temperature was also estimated from long-wave radiation data measured by the CNR1 sensor and the Stefan-Boltzmann equation (Oke, 1987):

$$\varepsilon\sigma {T_s}^4 = Q_{lw}\uparrow + (1-\varepsilon)Q_{lw}\downarrow \tag{6}$$

where σ is the Stefan-Boltzmann constant and ε is surface emissivity. Emissivity was assumed to be 0·98, which is a representative value for moss and lichen (Salisbury and D'Aria, 1992). The instrumental accuracy of the long-wave radiometer in the CNR1 sensor is estimated to be within 5 W m^{-2}, according to the manufacturer's specification, which is equivalent to 1 °C in surface temperature from Equation (6). In addition, an error in ε by 0·01 will cause approximately 1 °C error in the estimated surface temperature. Therefore, the overall accuracy of surface temperature measurement with the CNR1 sensor is expected to be within 2 °C. When the daily mean surface temperature during May and June 2004 were compared, the average difference between IRT sensor and the CNR1 sensor was +1·2 °C (IRT was higher) with a standard deviation of 0·8 °C. The difference was considered within the estimated instrumental error bounds.

Continuous cores of frozen peat, 7·4 cm in diameter and 70 cm in length, were collected using a gasoline-powered auger and core sampler near Centre Pit on 6 April 2003, before snowmelt started. The frozen cores were cut into 0·07–0·12 m sections and thawed in the laboratory to determine water content and dry bulk density by oven-drying and weighing.

Ground heat flux estimation

Ground heat flux Q_g (W m^{-2}) into the active layer consists of three components (Woo and Xia, 1996):

$$Q_g = Q_i + Q_s + Q_p \tag{7}$$

where Q_i (W m^{-2}) is the latent heat used to melt ice in the active layer, Q_s (W m^{-2}) is the heat that warms the active layer, and Q_p (W m^{-2}) is the heat conducted into the permafrost below. A number of methods are available for estimating Q_g, each having certain advantages and disadvantages (Sauer, 2002). Among commonly used methods, the flux-plate method is prone to errors due to the mismatch in thermal conductivity of the plate and the soil and poor contact between the plate and the soil (Halliwell and Rouse, 1987). Therefore, flux plates need to be calibrated using an independent method (van Loon *et al*., 1998). The gradient method requires an accurate estimate of soil thermal conductivity between the two temperature sensors measuring the thermal gradient. Several equations have been proposed to estimate soil thermal conductivity from the conductivity of individual phases (i.e. mineral, organic material, air, water, and ice) and their volume fractions (Farouki, 1981), but the accuracy of these methods for peat has not been tested extensively. The calorimetric method calculates Q_i from the rate of change in the frost table depth and the latent heat required to thaw the frozen soil, and Q_s from the rate of temperature change and the specific heat of the soil. The calorimetric method is very sensitive to estimates of ice content for Q_i and water content for Q_s (Halliwell and Rouse, 1987). The former is particularly important for wet, organic soil, where the majority of Q_g goes to Q_i, but the ice content cannot be easily measured by non-destructive methods. All three methods were used in this study in order to examine their consistency and increase the confidence in measured flux values.

The thermal conductivity λ (W m^{-1} °C^{-1}) of unfrozen peat was calculated using the equation of de Vries (1963):

$$\lambda = \frac{x_w\lambda_w + k_a x_a \lambda_a + k_s x_s \lambda_s}{x_w + k_a x_a + k_s x_s} \tag{8}$$

where x_w, x_a, and x_s are the volume fractions of water, air, and solid, respectively; λ_w, λ_a, and λ_s are thermal conductivities of water, air, and solid, respectively (Hillel, 1998, p. 316); and k_a and k_s are weighting factors given by:

$$k_a = \frac{1}{3}\left[\frac{2}{1+\left(\frac{\lambda_a}{\lambda_w}-1\right)g_a} + \frac{1}{1+\left(\frac{\lambda_a}{\lambda_w}-1\right)g_c}\right] \tag{9}$$

$$k_s = \frac{1}{3}\left[\frac{2}{1+\left(\frac{\lambda_s}{\lambda_w}-1\right)g_a} + \frac{1}{1+\left(\frac{\lambda_s}{\lambda_w}-1\right)g_c}\right] \tag{10}$$

DOI: 10.1002/hyp

$$g_a = 0{\cdot}333 - x_a(0{\cdot}333 - 0{\cdot}035)/m \quad (11)$$

$$g_c = 1 - 2g_a \quad (12)$$

and m is the porosity of peat. The accuracy of Equation (8) was examined by comparing the results with independently estimated λ from thermal diffusivity and volumetric heat capacity C (J m^{-3} °C^{-1}), where C was estimated from the specific heat and density of individual phases and their volume fractions (Hillel, 1998, p. 315). Thermal diffusivity was estimated from the harmonic analysis of diurnal temperature fluctuation (Horton *et al*., 1983).

For the calorimetric method (Woo and Xia, 1996), daily values of Q_i were calculated by

$$Q_i = \rho f L \Delta z \quad (13)$$

where Δz is the daily increase in the depth to the frost table. As in the present study, Woo and Xia (1996) assumed that the frost table (i.e. zero-degree isotherm) coincided with the cryofront (i.e. the melting upper surface of the frozen, saturated layer). This was verified by comparing direct measurements of the thickness of the thawed layer of soil using a frost probe, which detected the top of the frozen layer generally without any difficulty, with the depth to the zero-degree isotherm interpolated from the soil temperature data provided by the instrumented soil pit. To calculate Q_s, the active layer was partitioned into a number of computational layers representing the locations of the soil sensors. Daily values of Q_s were calculated by:

$$Q_s = \sum_i C_i d_i \Delta T_i \quad (14)$$

where C_i is the volumetric heat capacity, d_i (m) is the thickness, and ΔT_i (°C) is the daily temperature change of the i-th layer. Daily values of Q_p in Equation (7) were calculated from the thermal gradient and conductivity of frozen peat using Equation (8) with air replaced by ice (Farouki, 1981), assuming that little air exists in frozen peat. This assumption will be examined below with the results. The thermistors located at 0·5 and 0·7 m were used to estimate the thermal gradient at the bottom of the soil profile. In each thawing season, the analysis was terminated when the frost table reached a depth of 0·5 m because extrapolating the water content data at 0·4 m (deepest WCR) to depths below 0·5 m was deemed unreliable.

RESULTS

Soil thawing processes

In the following, 'water' is used to indicate liquid water and 'total moisture' is used to indicate the total of both liquid water and ice, unless otherwise stated. Snowmelt period lasted for 2–3 weeks, beginning in mid-April when the daily average air temperature rose above 0 °C (Figure 3(a)). Data from 2005 are used as an example to demonstrate soil thawing processes at the Centre Pit. Snow depth at the meteorological station was 0·8 m on 10 April 2005 when snow started melting (Figure 3(a)). Snowmelt was completed by 29 April at which time the soil began thawing from the ground surface, as indicated by the soil temperature (Figure 3(b)). Water content registered by the WCR was close to 0·2 at all depths while the soil was frozen (Figure 3(c)). While this may not indicate an accurate value of liquid water content without specific calibration (Spaans and Baker, 1996; Roth and Boike, 2001), similar methods have been used to estimate liquid water content (Romanovsky and Osterkamp, 2000). Therefore, pre-melt values measured by the WCR were used to represent liquid water remaining in frozen soil in

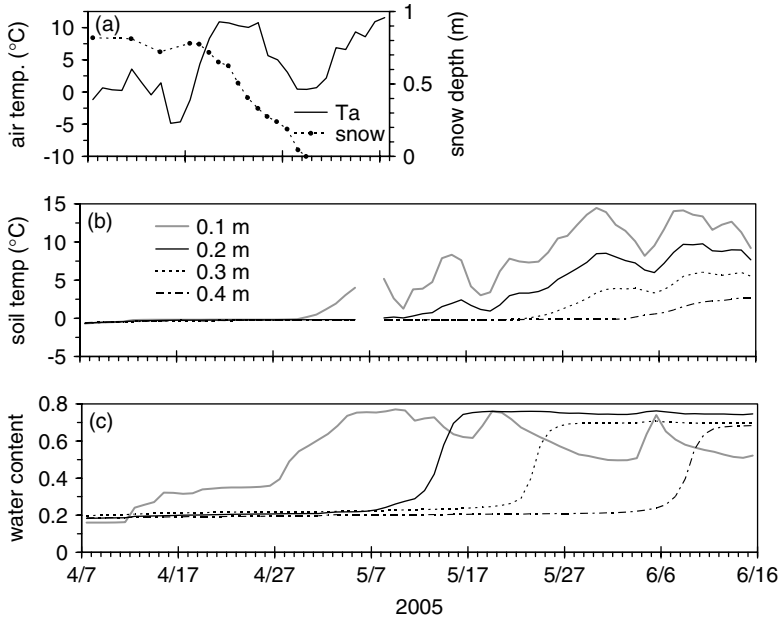

Figure 3. (a) Snow depth and daily average air temperature, (b) soil temperature, and (c) liquid water content in 2005 at Centre Pit

DOI: 10.1002/hyp

this study. Quinton *et al*. (2005) reported similar values of liquid water content (0·15–0·2) in frozen peat from the Wolf Creek Research Basin in Yukon Territories, Canada.

The WCR at 0·1 m indicated an increase in water content on 11 April (Figure 3(c)) at an early stage of snowmelt, while the soil at this depth was still largely frozen (Figure 3(b)). This likely indicates infiltration of snowmelt water in unsaturated soil (Stein and Kane, 1983). Some melt water probably re-froze in the soil as daily average air temperature (T_a) dropped significantly below 0 °C during 15–17 April (Figure 3(a)). The thawing front (i.e. frost table) reached 0·1 m on 30 April as indicated by the soil temperature data (Figure 3(b)), and the water content increased to near saturation indicating the phase change from ice to liquid (Figure 3(c)). The thawing front gradually descended as indicated by the increase in temperature (Figure 3(b)) and water content at 0·2, 0·3, and 0·4 m (Figure 3(c)). Similar patterns were observed in 2003 and 2004.

The total moisture content of the frozen soil cores sampled in 2003 (Figure 4(a)) was close to porosity at depths greater than 0·25 m, implying that the peat below 0·25 m was frozen under saturated conditions. Core 1 was sampled from moss-covered ground, and Core 2 from lichen-covered ground. The moss profile had much higher total moisture content than the lichen profile in the top 0·25 m (Figure 4(a)). Figure 4(b) shows volumetric water content measured by the WCR just before the soil started freezing at each depth (late September to early November). The soil was very wet below 0·2 m, but the water content was slightly below saturation. The difference between Figure 4(a) and (b) may be explained by spatial variability or by liquid and vapour transfer processes during freeze-up.

The calorimetric method of heat-flux calculation requires an estimate of the volumetric fraction of individual phases in the soil. On the basis of the porosity distribution (Figure 2), the total pre-melt moisture content (Figure 4(a)), and the pre-melt value of the liquid water content measured by the WCR (e.g. Figure 3), depth profiles of individual phases shown in Figure 4(c) were used for the calorimetric calculation in 2003. For 2004 and 2005, liquid water contents were adjusted according to the pre-melt WCR data, but the 2003 data were used for organic material and air content because frozen cores were only sampled in 2003. Total moisture content of frozen soil in 2004 and 2005 is expected to be similar to that in 2003 because the pre-freezing water content profiles were similar in all 3 years (Figure 4(b)).

Thermal diffusivity and conductivity

Thermal diffusivity was determined by the harmonic analysis of one-dimensional heat conduction (Horton *et al*., 1983). The standard method assumes that the soil is homogeneous and infinitely deep. Such an assumption is rarely satisfied in the field, resulting in significant over- or under-estimation of diffusivity (e.g. Passerat de Silans *et al*., 1996). In order to make a preliminary assessment of the homogeneous soil assumption, soil thermal conductivity at Centre Pit was estimated using Equation (8) from porosity (Figure 2) and monthly average water content data in June 2005; and thermal diffusivity was calculated from conductivity and volumetric heat capacity (Figure 5). Thermal diffusivity was reasonably uniform throughout the profile but conductivity and heat capacity changed dramatically in the top 0·2 m, suggesting that the standard method may not work in this zone (Massman, 1993).

To investigate this issue further, the one-dimensional heat conduction equation with the soil thermal property shown in Figure 5 was solved numerically using a finite-difference method:

$$C(z)\frac{\partial T}{\partial t} = \frac{\partial}{\partial z}\left(\lambda(z)\frac{\partial T}{\partial z}\right) \tag{15}$$

The bottom boundary was assumed to be located at a depth of 0·6 m, and temperature T at the top boundary was given by a cosine function having a period of one day. Equation (15) and the boundary conditions were Fourier-transformed and solved in the frequency domain using a method similar to Townley (1995). The amplitude of temperature oscillation at each node was used to compute apparent thermal diffusivity (Nassar and Horton, 1989) for each layer (Figure 5(c)). The apparent thermal diffusivity estimated from the harmonic analysis was significantly different from the actual thermal diffusivity in the top 0·2 m as expected, but matched closely below

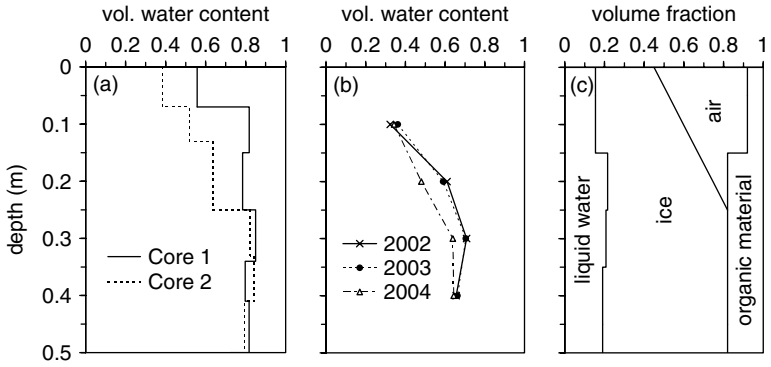

Figure 4. (a) Total volumetric moisture content of frozen peat cores. (b) Volumetric water content prior to freezing. (c) Volumetric fraction of individual phases used in the calorimetric method

DOI: 10.1002/hyp

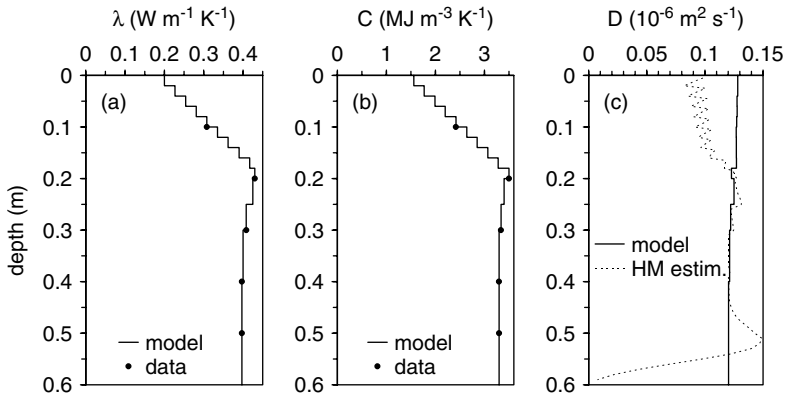

Figure 5. Profiles of (a) thermal conductivity, (b) volumetric heat capacity, and (c) thermal diffusivity. Solid circles in (a) and (b) indicate estimated values based on the average soil temperature and moisture content data in June 2005. Solid lines indicate the values used in numerical simulation. Dashed line in (c) indicates the diffusivity values calculated from simulated amplitude of fluctuation using the harmonic analysis (HM)

0·2 m except near the bottom boundary due to the reflection of the thermal wave (Karam, 2000). These results indicate that the standard harmonic analysis can be applied to field-measured temperature below 0·2 m when the frost table is located more than 0·1–0·15 m below the depth of measurement.

The harmonic analysis was applied to temperature measured at 0·2 and 0·25 m in Centre Pit for individual 10-day periods in June–August 2004 and 2005 to monitor seasonal changes in thermal properties. The temperature signal for each 10-day period was first de-trended by subtracting the 24-h moving average values from the original data (see Figure 6 for example), and then the de-trended signals were Fourier-transformed to extract the diurnal component. Only the amplitude of diurnal fluctuation was used to compute thermal diffusivity (Horton *et al*., 1983, Equation (6)) because the sampling interval (hourly in 2004 and half-hourly in 2005) was too coarse to determine the phase lag accurately. Thermal conductivity was calculated by multiplying diffusivity with the volumetric heat capacity estimated from porosity and water content. Conductivity values plotted in Figure 7 have a range indicated by a bar to reflect the uncertainty in the distance between the two thermistors (4·75–5·25 cm, where it was designed to be 5 cm). Thermal conductivity varied between 0·3 and 0·4 W m^{-1} $°C^{-1}$ in both summers. Values predicted by Equation (8) were reasonably close to measured values (Figure 7), indicating that Equation (8) can be reliably used at the study site.

The air conductivity term (λ_a) in Equation (8) is an apparent thermal conductivity that includes the effects of heat transfer associated with vapour diffusion in air-filled pore spaces (Kane *et al*., 2001). This term is strongly dependent on temperature and may affect the overall soil thermal conductivity. Campbell *et al*. (1994, Equation 11) proposed a modification to Equation (8), which explicitly accounted for the temperature dependence of λ_a. Comparison of the equations by de Vries (1963) and Campbell *et al*. (1994) showed little difference between the two (Figure 7) because λ_a plays a minor role in this wet environment. Therefore, the computationally simpler de Vries (1963) equation with a constant λ_a is used in the following analysis.

Calibration of the heat-flux plate and evaluation of the calorimetric method

In order to calibrate the heat-flux plate, located 0·05 m below the surface, ground heat flux (Q_g) was calculated by adding the calorimetrically estimated heat storage between 0 and 0·05 m to the flux-plate reading (Mayocchi and Bristow, 1995) for June August 2004 and 2005. Q_g

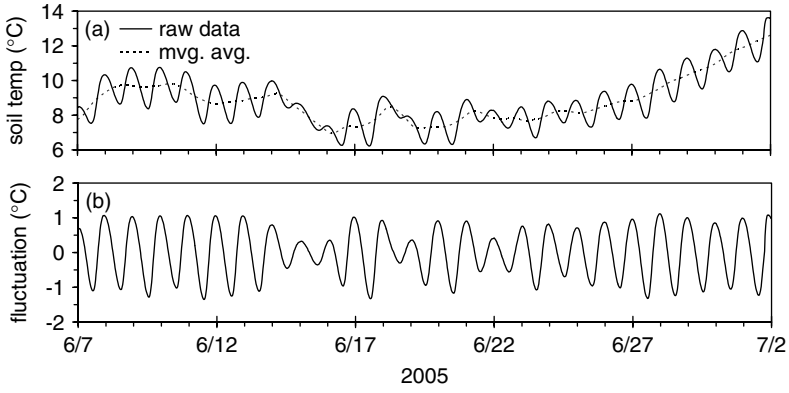

Figure 6. (a) Raw soil temperature data and 24-h moving average at 0·2 m depth in June 2005. (b) De-trended data given by the difference between the raw data and the moving average

DOI: 10.1002/hyp

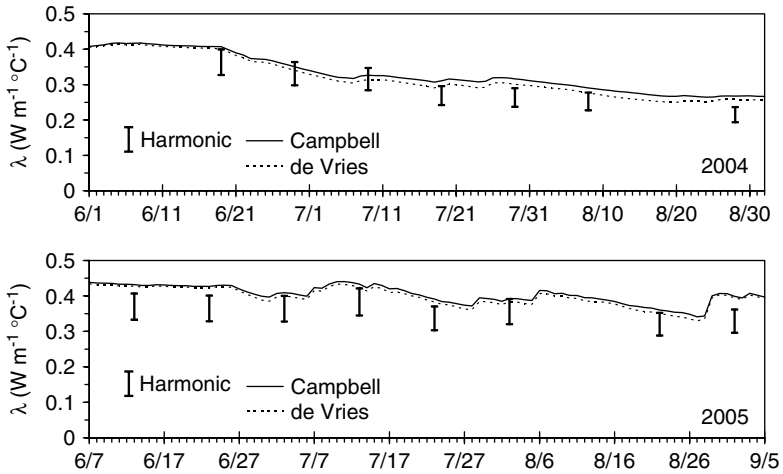

Figure 7. Thermal conductivity estimated by applying the harmonic method for 10-day periods, assuming $\Delta z = 4{\cdot}75-5{\cdot}25$ cm. Continuous lines indicate daily values of thermal conductivity estimated by the equations of Campbell *et al.* (1994) and de Vries (1963)

was also calculated for the same periods from the thermal gradient between 0·2 and 0·25 m, the thermal conductivity using Equation (8), and the calorimetrically estimated heat storage between 0 and 0·2 m. Five-day average values were computed for the two methods to remove noises resulting from the sensitivity of the calorimetric calculation to short-term temperature fluctuation. The flux plate underestimated Q_g in both years compared to the gradient method (Figure 8), which is consistent with reports by previous workers (e.g. Halliwell and Rouse, 1987). By fitting a straight line to the data points by the least-squares method (Figure 8), a linear calibration factor of 1·33 was determined.

Compared to the gradient and the flux-plate methods, the calorimetric method has an advantage of being able to determine Q_i, Q_s, and Q_p individually, but it is highly sensitive to errors in estimating ice content in the soil. In order to assess the accuracy of the calorimetric method, Q_g measured by the calibrated flux plate was compared against Q_g estimated by the calorimetric method in 2004 and 2005, starting when the frost table reached the depth of the heat flux plate. Q_g measured by the two methods was generally in good agreement although there were some day-to-day variations (Figure 9). Average values of flux-plate Q_g and calorimetric Q_g were 25·1 and 22·8 W m^{-2}, respectively, in 2004; and 23·9 and 24·1 W m^{-2}, respectively, in 2005; indicating that we can treat the calorimetric data with a reasonable degree of confidence.

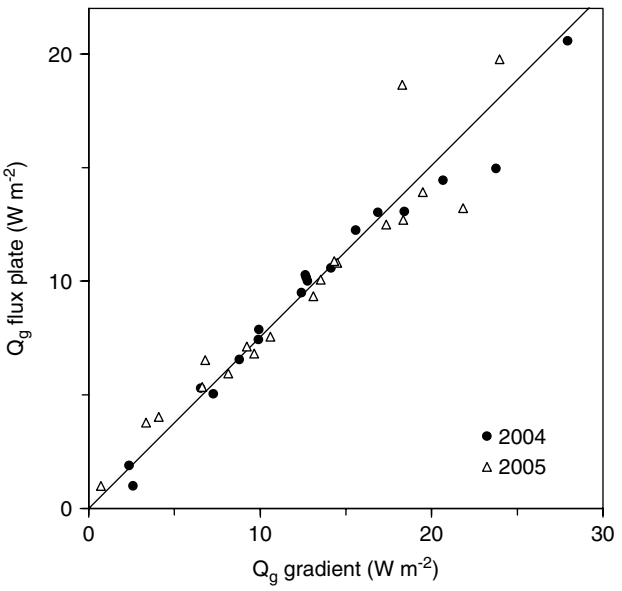

Figure 8. Comparison of 5-day average ground heat flux (Q_g) measured with the heat flux plate and estimated by the gradient method

Performance evaluation of the heat-conduction method

In order to assess the validity of the first assumption used to derive Equation (3), the cumulative total of the three flux components (Q_i, Q_s, and Q_p) was calculated for the thawing observation periods of 2003, 2004, and 2005 using the Centre Pit data (Table I). The ground heat flux was dominated by the latent heat used to melt the ice (Q_i) which accounted for at least 86% of the total, while the heat used to warm the soil column (0–0·5 m) (Q_s) accounted for 9–12% and the heat conducted into the frozen soil below (Q_p) was almost negligible. Therefore, it is acceptable to assume that the majority of Q_g is used to thaw the ice at the frost table. Cumulative net radiation (R_n) over the periods was 494 MJ m^{-2} and 452 MJ m^{-2} in 2004 and 2005, respectively. (Table I). Cumulative ground heat flux (Q_g) was 19–21% of cumulative R_n (Table I), which is comparable to previous studies in similar environments (Carey and Woo, 2000; Quinton *et al.*, 2005).

The soil temperature profile at any given time was not a straight line as assumed in Equation (3) due to the propagation of surface-temperature fluctuations. However, when averaged over several days, the temperature profile was reasonably linear regardless of the depth to the frost table (Figure 10). Therefore, the assumption of a linear-temperature profile is justified for simulating the seasonal propagation of the frost table, where short-term variations are averaged out (Equation (4)).

DOI: 10.1002/hyp

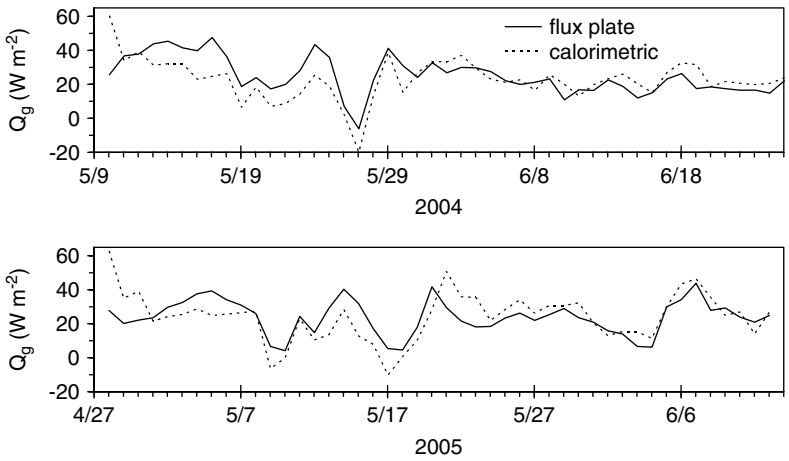

Figure 9. Comparison of the ground heat flux (Q_g) measured by the flux plate and the calorimetric method

Table I. Total precipitation (P), cumulative total of the latent heat used to melt the ice (Q_i), the heat that warms the soil column (Q_s), the heat conducted into the permafrost below (Q_p), ground heat flux (Q_g), net radiation (R_n); average Q_i/Q_g and Q_g/R_n, and the n-factor for the thawing periods of 2003–2005. Note that the analysis ended when the frost table reached a depth of 0·5 m

Year	Period	P mm	Qi MJ m^{-2}	Qs MJ m^{-2}	Qp MJ m^{-2}	Qg MJ m^{-2}	Rn MJ m^{-2}	Qi/Qg	Qg/Rn	n
2003	Apr. 26–Jun. 26	104	82·6	8·0	2·9	93		0·88		0·97
2004	May 9–Jun. 25	71	80·9	10·8	0·97	93	494	0·87	0·19	0·95
2005	Apr. 27–Jun. 12	61	82·4	11·6	1·8	96	452	0·86	0·21	1·02

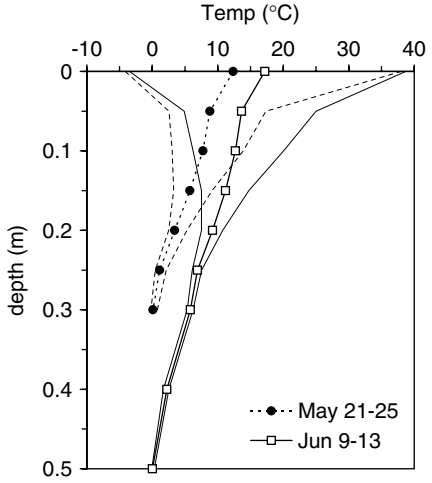

Figure 10. Examples of soil temperature profile in 2005. Values at 0 m indicate surface temperature (T_s). Five-day average values are shown by symbols and thick lines, and half-hourly maximum and minimum values during the 5-day period are shown by thin lines. The frost table was located at 0·3 m on 23 May and 0·5 m on 11 June

The integral form of the heat-conduction method (Equation (4)) was applied to the Centre Pit data for 2003, 2004, and 2005. The bulk thermal conductivity (λ_b) was given by the harmonic average of the thermal conductivity of individual layers between the ground surface and the frost table. The thermal conductivity of individual layers was calculated using Equation (8). Daily average surface temperature was mostly at or above 0 °C, except during 2–4 May, 2005. The depth to the frost table linearly increased with the square root of the product of the daily average thermal conductivity and surface temperature in all 3 years of observation (Figure 11(a)). The best-fit value of α in Equation (4), determined by the least-squares method, was $1{\cdot}18 \times 10^{-4}$ J$^{-1/2}$ m$^{3/2}$. If Equation (4) provides a good representation of heat conduction, it should also work with temperature measured at an arbitrary depth, using that depth as the top boundary condition. To test this idea, Equation (4) is slightly modified to:

$$z = z_0 + \alpha(86\,400\Sigma\lambda_b T_{z0})^{1/2} \qquad (16)$$

where z_0 is the depth of the temperature measurement and T_{z0} is the soil temperature at z_0. Taking $z_0 = 0{\cdot}05$, the frost table depth linearly increased with $(86\,400\ \Sigma\lambda_b T_{z0})^{1/2}$ in all 3 years (Figure 11(b)). The best-fit value of α was $1{\cdot}20 \times 10^{-4}$ J$^{-1/2}$ m$^{3/2}$, which was very close to the value for the surface-temperature case (Figure 11(a)).

In the calorimetric calculation above, the average ice content (f) of the 0·5 m profile (Figure 4(c)) was estimated to be 0·54 based on the measurements on the two frozen peat cores. Using $f = 0{\cdot}54$, ice density (ρ) of 890 kg m^{-3}, and latent heat (L) of $3{\cdot}34 \times 10^5$ J kg^{-1}, Equation (5) predicts α of $1{\cdot}12 \times 10^{-4}$ J$^{-1/2}$ m$^{3/2}$. This is reasonably close to the empirically determined value of $1{\cdot}18 \times 10^{-4}$ J$^{-1/2}$ m$^{3/2}$, suggesting that Equation (4) simulated the seasonal progression of the frost table reasonably well. Therefore, the simple heat-conduction method (Equation (3)) will provide a useful algorithm for simulating the frost table depth without site-specific

DOI: 10.1002/hyp

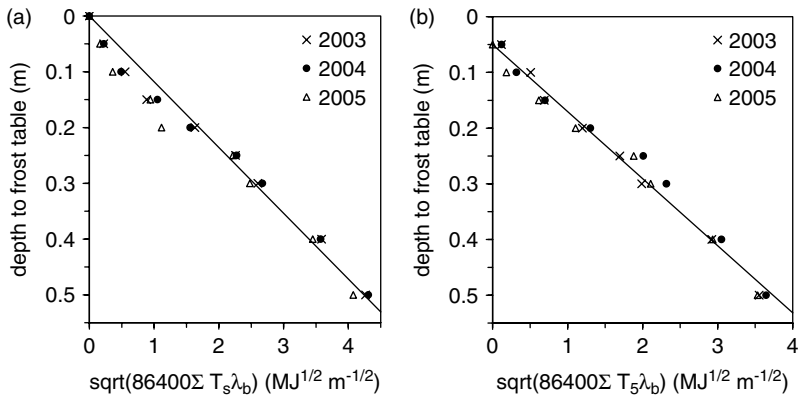

Figure 11. Relation between the frost table depth and the cumulative product of bulk thermal conductivity (λ_b) and; (a) surface temperature (T_s), (b) soil temperature at 0·05 m (T_5). Solid lines show Equations (4) and (16) with the least-squares fit values of α

calibration if physical parameters, such as thermal conductivity and ice content, are known with a reasonable degree of accuracy.

Inter-site transferability

Transferability of Equation (4) to different sites was examined by applying it to West Pit with $\alpha = 1{\cdot}18 \times 10^{-4}$ J$^{-1/2}$ m$^{3/2}$. Temperature measured by the 0·05 m thermistor (T_5) was used with Equation (16) because surface temperature data were not available for West Pit. Bulk thermal conductivity was estimated using the water content measured by the 0·2 m WCR to represent the entire thawed layer because only one WCR was installed in the pit. The frost table depths simulated by Equations (4) and (16) were reasonably close to the observed data for both pits in 2004 (Figure 12(a)). Similar results were obtained for 2003 and 2005.

Since the Centre and West Pits are separated by only 14 m, the meteorological conditions (e.g. air temperature and incoming radiation) over the two sites are expected to be nearly identical. Similar values of albedo were measured for the two major land-cover types, moss (0·15) and lichen (0·19), on 3 September 2006 using two identical pyranometers (Kipp & Zonen, CMP3), facing up and down, placed 0·4 m above the ground surface under a thin cloud cover with short-wave incoming radiation ranging 100–200 W m^{-2}. Despite the very similar meteorological forcing, the thawing rate at West Pit was much lower than the thawing rate at Centre Pit (Figure 12(a)). Equation (4) suggests that the dramatic difference in thawing rates between the two sites is due to differences in surface temperature and thermal conductivity, the latter being strongly dependent on water content. In order to assess the effects of surface temperature, soil temperature at 0·05 m was compared between the two sites in 2004. Temperature was much lower at West Pit than Centre Pit until early June, but the difference became relatively small afterwards (Figure 12(b)), suggesting that surface temperature is not the primary cause of difference in thawing rates. Liquid water content at 0·2 m increased sharply after the thawing of this depth by mid-May in Centre Pit and

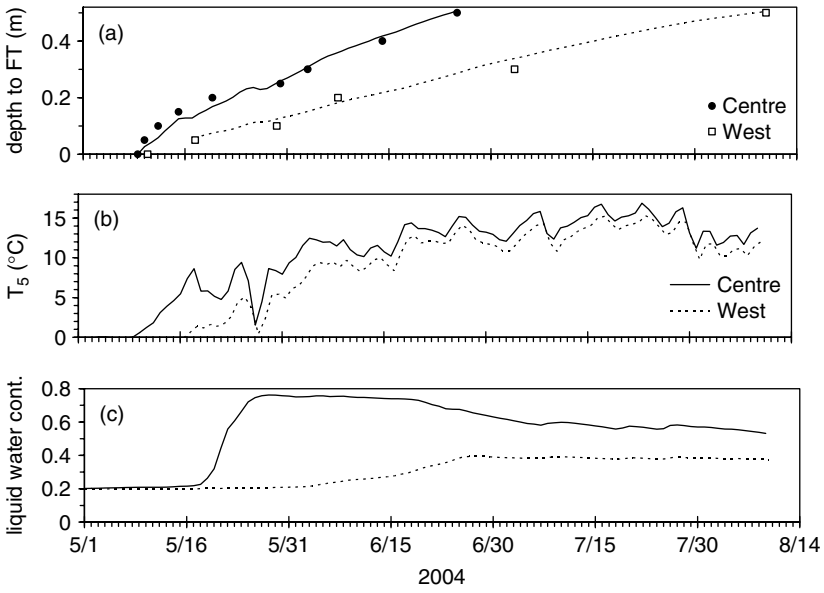

Figure 12. Comparison of Centre and West Pit in 2004. (a) Measured (symbols) and simulated frost table (FT) depth. (b) Soil temperature at 0·05-m depth. (c) Liquid water content measured by the water content reflectometer at 0·2-m depth

DOI: 10.1002/hyp

by mid-June in West Pit (Figure 12(c)). The post-thaw water content was much lower in West Pit than in the Centre Pit, resulting in a large difference in bulk thermal conductivity, which was the primary factor responsible for the difference in thawing rates. This is consistent with previous studies that showed that the thickness of the active layer was strongly dependent on moisture conditions (Nelson *et al*., 1997; Kane *et al*., 2001; Hinkel and Nelson, 2003).

DISCUSSION

Effects of non-conductive processes

The heat-conduction method to simulate the lowering of the frost table (Equation (3)) ignores the heat used to warm the active layer (Q_s). Although Q_s was indeed much smaller than the latent heat (Q_i) used to melt ice in the soil (Table I), it still accounts for roughly 10% of ground heat flux. The fact that the empirically determined α in Equation (4) was close to the theoretical value predicted by Equation (5) implies that non-conductive processes, such as infiltration, may have contributed to offset the loss of energy to Q_s (Romanovsky and Osterkamp, 2000; Kane *et al*., 2001). During the 2003 thawing period (26 April–26 June) total rainfall was 104 mm (Table I) and average surface temperature was 10·2 °C. Assuming that the temperature of rain water infiltrating into the ground is equal to the surface temperature, a crude estimate of cumulative heat added to the ground by rainfall is given by:

$$0{\cdot}104\ \text{m} \times 4{\cdot}2\ \text{MJ m}^{-3}\ {}^{\circ}\text{C}^{-1} \times 10{\cdot}2\ {}^{\circ}\text{C} = 4{\cdot}5\ \text{MJ m}^{-2}$$

where the second term in the left-hand side of the equation is volumetric heat capacity of water. This is much smaller than cumulative Q_s in 2004 (Table I), suggesting that infiltration alone may be insufficient to balance Q_s.

Potential application of the heat-conduction method

The heat-conduction method was successfully applied to simulate the frost table depth at two different locations within the study site (Figure 12(a)). If realistic estimates of peat porosity and the thermal conductivity of the organic matter are available, this method will provide a computationally efficient frost table algorithm to be used in hydrological models that compute surface temperature and liquid and solid water contents as state variables. A relatively small number (<10) of peat profile samples are probably sufficient to characterize the porosity and thermal conductivity of the organic matter, because these parameters do not vary appreciably owing to the common botanical origin of the peat on the plateau (Quinton and Hayashi, 2005). In addition, the method will be useful for examining the factors controlling the spatial variability of frost table depths over a hillslope scale (Nelson *et al*., 1997; Metcalfe and Buttle, 1999). For example, the equation can demonstrate the dependence of frost table depth on the wetness of the soil, which may be influenced by micro-topography or vegetation cover. The 'topography' of the relatively impermeable frost table thus formed may strongly influence the drainage of hillslopes (Tromp-van Meerveld and McDonnell, 2005).

Large-scale application of the method will require estimates of physical parameters based on information on land cover and soil types. When the parameter values are not readily available, the method may be applied with empirically determined values of α, based on previous studies on active layer thickness. Comparing Equations (2)–(4), it follows that:

$$\alpha = \beta/(n\lambda_b)^{1/2} \tag{17}$$

Anisimov *et al*. (2002) compiled an extensive data set from the Kuparuk River region of north-central Alaska, USA, and reported class-mean values of β ranging from 1·7 and 2·1 cm $\text{d}^{-1/2}$ $^{\circ}\text{C}^{-1/2}$ for four vegetation classes representing relatively dry areas, probably somewhat similar to the peat plateau examined in this study. Seasonal average values of n-factor were close to unity at Scotty Creek (Table I), while the values reported in the previous literature range from 0·7 to 1·1 (e.g. Klene *et al*., 2001; Karunaratne and Burn, 2004). Assuming $n = 1$ and bulk thermal conductivity of 0·3–0·4 W m^{-1} $^{\circ}\text{C}^{-1}$ (Figure 7), Equation (7) gives $\alpha = 0{\cdot}9\text{–}1{\cdot}1 \times 10^{-4}$ $\text{J}^{-1/2}$ $\text{m}^{3/2}$ for $\beta = 1{\cdot}7$ cm $\text{d}^{-1/2}$ $^{\circ}\text{C}^{-1/2}$, and $\alpha = 1{\cdot}2\text{–}1{\cdot}4 \times 10^{-4}$ $\text{J}^{-1/2}$ $\text{m}^{3/2}$ for $\beta = 2{\cdot}1$ cm $\text{d}^{-1/2}$ $^{\circ}\text{C}^{-1/2}$. The calculated values of α are reasonably close to the observed value ($1{\cdot}2 \times 10^{-4}$ $\text{J}^{-1/2}$ $\text{m}^{3/2}$) at our site, suggesting that it may be feasible to use the literature data to estimate α.

CONCLUSIONS

In a peat plateau underlain by permafrost in northwestern Canada, the majority (>86%) of ground heat flux in summer was used to melt ice in the frozen peat. The soil temperature profile between the ground surface and the thawing front was linear when averaged over several days, indicating that ground heat flux can be modelled using a simple heat conduction equation assuming a linear temperature gradient. An integral form of the simple heat conduction equation, similar to the Stefan equation, was used with field-measured physical parameters to simulate the seasonal progression (i.e. downward movement) of the frost table with reasonable accuracy. The results were transferable between two locations on the peat plateau without site-specific calibration. The heat conduction model clearly showed that a large difference in thawing rates between the two locations is primarily due to the difference in their soil moisture condition. The method is physically based, and can easily be incorporated into hydrological models that compute ground surface temperature and soil water content as state variables. Therefore, it might provide a useful tool for simulating hillslope drainage in organic-covered permafrost terrains and for evaluating the effects of topography and land

DOI: 10.1002/hyp

cover on the temporal and seasonal variability of the frost table.

Three different methods (gradient, calorimetric, and flux plate) were used to estimate the ground heat flux in this study, all of which provided consistent results, giving a high degree of confidence in the heat-flux data that were used to test the model. Furthermore, the thermal conductivity computed from theoretical equations matched the field-based estimates, indicating that these equations give reasonably good results in organic soil. Accurate estimation of the ice content in frozen soil is important for the simulation of the frost table depth and for the calorimetric method of computing the ground heat flux, because both are highly sensitive to ice content.

ACKNOWLEDGEMENT

We thank Roger Pilling and Gerry Wright of the Water Survey of Canada for logistical support; and Michael Toews, Jaclyn Schmidt, Cuyler Onclin, and Greg Langston for their field assistance. Logistical support was also provided by the National Hydrology Research Centre of Environment Canada. This study was made possible through the support of the Deh Cho First Nation, Denendeh Resource Committee, Fort Simpson Metis Local #52, Liidlii Kue First Nation, and the Village of Fort Simpson. Funding was provided by the Natural Sciences and Engineering Research Council of Canada, the Canadian Foundation for Climate and Atmospheric Science, Environment Canada Science Horizons Program, and the Northern Science Training Program. Constructive comments by two anonymous reviewers greatly improved the manuscript.

APPENDIX

Suppose that $z = 0$ at $t = 0$. Separating variables in Equation (3) and integrating them with respect to time from 0 to t yields:

$$\frac{z^2}{2} = \frac{1}{\rho f L}\int_0^t \lambda_b(\tau)T_s(\tau)d\tau \qquad [A1]$$

Multiplying both sides of Equation (A1) by 2 and taking square roots gives:

$$z(t) = \sqrt{\frac{2}{\rho f L}\int_0^t \lambda_b(\tau)T_s(\tau)d\tau} \qquad [A2]$$

Note that the integral can be approximated by

$$\int_0^t \lambda_b(\tau)T_s(\tau)d\tau \cong 86\,400\sum_i \lambda_{bi}T_{si} \qquad [A3]$$

where λ_{bi} and T_{si} are daily average values of bulk thermal conductivity and surface temperature, respectively on the i-th day. Substituting Equation (A3) into Equation (A2) yields Equation (4).

REFERENCES

Anisimov OA, Shiklomanov NI, Nelson FE. 2002. Variability of seasonal thaw depth in permafrost regions: a stochastic modeling approach. *Ecological Modelling* **153**: 217–227.

Aylesworth JM, Kettles IM. 2000. Distribution of peatlands. In *The Physical Environment of the Mackenzie Valley, Northwest Territories: A Base Line for the Assessment of Environmental Change*, Dyke LD, Brooks GR (eds). Natural Resources Canada, Ottawa *Geological Survey of Canada Bulletin 547*; 49–55.

Beckwith CW, Baird AJ, Heathwaite AL. 2003. Anisotropy and depth-related heterogeneity of hydraulic conductivity in a bog peat. I: laboratory measurements. *Hydrological Processes* **17**: 89–101.

Burgess MM, Smith SL. 2000. Shallow ground temperatures. In *The Physical Environment of the Mackenzie Valley, Northwest Territories: A Base Line for the Assessment of Environmental Change*, Dyke LD, Brooks GR (eds). Natural Resources Canada, Ottawa. *Geological Survey of Canada Bulletin, 547*: 89–103.

Campbell GS, Jungbauer JD Jr. Bidlake WR, Hunger ford RD. 1994. Predicting the effect of temperature on soil thermal conductivity. *Soil Science* **158**: 307–313.

Carey SK, Woo M-K. 2000. Within-slope variability of ground heat flux, subarctic Yukon. *Physical Geography* **21**: 407–417.

Chason DB, Siegel DI. 1986. Hydraulic conductivity and related physical properties of peat, Lost River Peatland, northern Minnesota. *Soil Science* **142**: 91–99.

Cherkauer KA, Lettenmaier DP. 1999. Hydrologic effects of frozen soils in the upper Mississippi River basin. *Journal of Geophysical Research* **104**(D16): 19,599–19,610.

Farouki OT. 1981. The thermal properties of soils in cold regions. *Cold Regions Science and Technology* **5**: 67–75.

Halliwell DH, Rouse WR. 1987. Soil heat flux in permafrost: characteristics and accuracy of measurement. *Journal of Climatology* **7**: 571–584.

Hayashi M, Quinton WL, Pietroniro A, Gibson JJ. 2004. Hydrologic functions of wetlands in a discontinuous permafrost basin indicated by isotopic and chemical signatures. *Journal of Hydrology* **216**: 81–97.

Hillel D. 1998. *Environmental Soil Physics*. Academic Press: San Diego, CA.

Hinkel KM, Nelson FE. 2003. Spatial and temporal patterns of active layer thickness at Circumpolar Active Layer Monitoring (CALM) sites in northern Alaska, 1995–2000. *Journal of Geophysical Research* **108**(D2): 8168, doi:10·1029/2001JD000927.

Hinkel KM, Nicholas JRJ. 1995. Active layer thaw rate at a boreal forest site in central Alaska, U.S.A. *Arctic and Alpine Research* **27**: 72–80.

Horton R, Wierenga PJ, Nielsen DR. 1983. Evaluation of methods for determining the apparent soil thermal diffusivity of soil near the surface. *Soil Science Society of America Journal* **47**: 25–32.

Jumikis AR. 1977. *Thermal Geotechnics*. Rutgers University Press; New Brunswick, New Jersey. 375.

Kane DL, Hinkel KM, Goering DJ, Hinzman LD, Outcalt SI. 2001. Non-conductive heat transfer associated with frozen soils. *Global and Planetary Change* **29**: 275–292.

Karam MA. 2000. A thermal wave approach for heat transfer in a nonuniform soil. *Soil Science Society of America Journal* **64**: 1219–1225.

Karunaratne KC, Burn CR. 2004. Relations between air and surface temperature in discontinuous permafrost terrain near Mayo, Yokon Territory. *Canadian Journal of Earth Science* **41**: 1437–1451.

Klene AE, Nelson FE, Shiklomanov NI, Hinkel KM. 2001. The n-factor in natural landscapes: Variability of air and soil-surface temperatures, Kuparuk River Basin, Alaska, U.S.A. *Arctic, Antarctic, and Alpine Research* **33**: 140–148.

van Loon WKP, Bastings HMH, Moors EJ. 1998. Calibration of soil heat flux sensors. *Agricultural and Forest Meteorology* **92**: 1–8.

Massman WJ. 1993. Periodic temperature variations in an inhomogeneous soil: A comparison of approximate and exact analytical expressions. *Soil Science* **155**: 331–338.

Mayocchi CL, Bristow KL. 1995. Soil surface heat flux: some general questions and comments on measurements. *Agricultural and Forest Meteorology* **75**: 43–50.

Metcalfe RA, Buttle JM. 1999. Semi-distributed water balance dynamics in a small boreal forest basin. *Journal of Hydrology* **226**: 66–87.

Meteorological Service of Canada (MSC). 2002. *National Climate Data Archive of Canada*. Environment Canada: Dorval, Quebec.

Nelson FE, Outcalt SI. 1987. A computational method for prediction and regionalization of permafrost. *Arctic and Alpine Research* **19**: 279–288.

Nelson FE, Shiklomanov NI, Mueller GR, Hinkel KM, Walker DA, Bockheim JG. 1997. Estimating active-layer thickness over a large

region: Kuparuk River basin, Alaska, U.S.A. *Arctic and Alpine Research* **29**: 367–378.

Nassar IN, Horton R. 1989. Determination of the apparent thermal diffusivity of a nonuniform soil. *Soil Science* **147**: 238–244.

Oke TR. 1987. *Boundary layer climates*, 2nd ed. Routledge: London; 435.

Passerat de Silans AMB, Monteny BA, Lhomme JP. 1996. Apparent soil thermal diffusivity, a case study: HAPEX-Sahel experiment. *Agricultural and Forest Meteorology* **81**: 201–216.

Quinton WL, Marsh P. 1999. A conceptual framework for runoff generation in a permafrost environment. *Hydrological Processes* **13**: 2563–2581.

Quinton WL, Gray DM. 2001. Estimating subsurface drainage from organic-covered hillslopes underlain by permafrost: toward a combined heat and mass flux model. In *Soil-vegetation-atmosphere transfer schemes and large-scale hydrological models. Sixth IAHS scientific assembly*, Maastricht, Netherlands, 333–341.

Quinton WL, Hayashi M. 2005. The flow and storage of water in the wetland-dominated central Mackenzie river basin: recent advances and future directions. In *Prediction in Ungauged Basins: Approaches for Canada's Cold Regions*, Spence C, Pomeroy JW, Pietroniro A (eds). Canadian Water Resources Association: 45–66.

Quinton WL, Gray DM, Marsh P. 2000. Subsurface drainage from hummock-covered hillslope in the Arctic tundra. *Journal of Hydrology* **237**: 113–125.

Quinton WL, Hayashi M, Pietroniro A. 2003. Connectivity and storage functions of channel fens and flat bogs in northern basins. *Hydrological Processes* **17**: 3665–3684.

Quinton WL, Shirazi T, Carey SK, Pomeroy JW. 2005. Soil water storage and active-layer development in a sub-alpine tundra hillslope, southern Yukon Territory, Canada. *Permafrost and Periglacial Processes* **16**: 369–382.

Robinson SD, Moore TR. 1999. Carbon and peat accumulation over the past 1200 years in a landscape with discontinuous permafrost. *Global Biogeochemical Cycles* **13**: 591–601.

Romanovsky VE, Osterkamp TE. 2000. Effects of unfrozen water on heat and mass transport processes in the active layer and permafrost. *Permafrost and Periglacial Processes* **11**: 219–239.

Roth K, Boike J. 2001. Quantifying the thermal dynamics of a permafrost site near Ny-Ålesund, Svalbard. *Water Resources Research* **37**: 2901–2914.

Roulet NT, Woo M-K. 1986. Hydrology of a wetland in the continuous permafrost region. *Journal of Hydrology* **89**: 73–91.

Salisbury JW, D'Aria DM. 1992. Emissivity of terrestrial materials in the 8–14 μm atmospheric window. *Remote Sensing of Environment* **42**: 83–106.

Sauer TJ. 2002. Heat flux density. In *Methods of Soil Analysis, Part 4. Physical Methods*. *Soil Science Society of America Book Series 5*, Dane JH, Topp GC(eds). Madison, Wisconsin; 1233–1248.

Shur Y, Hinkel KM, Nelson FE. 2005. The transient layer: implication for geocryology and climate-change science. *Permafrost and Periglacial Processes* **16**: 5–17.

Soil Classification Working Group (SCWG). 1998. *The Canadian System of Soil Classification*, 3rd ed. Agriculture and Agri-Food Canada Publication 1646, Ottawa, 187.

Spaans EJA, Baker JM. 1996. The soil freezing characteristic: its measurement and similarity to the soil moisture characteristic. *Soil Science Society of America Journal* **60**: 13–19.

Stein J, Kane DL. 1983. Monitoring the unfrozen water content of soil and snow using time domain reflectometry. *Water Resources Research* **19**: 1573–1584.

Townley LR. 1995. The response of aquifers to periodic forcing. *Advances in Water Resources* **18**: 125–146.

Tromp-van Meerveld HJ, McDonnell JJ. 2006. Threshold relations in subsurface stormflow: 2. The fill and spill hypothesis. *Water Resources Research* **42**: W02411. DOI: 10·1029/2004WR003800.

Verseghy DL, McFarlane NA, Lazare M. 1993. CLASS—a Canadian land surface scheme for GCMs, II. Vegetation model and coupled runs. *International Journal of Climatology* **13**: 347–370.

de Vries DA. 1963. Thermal properties of soil. In *Physics of Plant Environment*. van Dijk WR (ed). North Holland Publishing: Amsterdam; 210–235.

Woo M-K. 1986. Permafrost hydrology in North America. *Atmosphere-Ocean* **24**: 201–234.

Woo M-K, Winter TC. 1993. The role of permafrost and seasonal frost in the hydrology of northern wetlands in North America. *Journal of Hydrology* **141**: 5–31.

Woo M-K, Xia Z. 1996. Effects of hydrology on the thermal conditions of the active layer. *Nordic Hydrology* **27**: 429–448.

Zhang Z, Kane DL, Hinzman LD. 2000. Development and application of a spatially-distributed Arctic hydrological and thermal process model (ARHYTHM). *Hydrological Processes* **14**: 1017–1044.

Zhao L, Gray DM, Male D. 1997. Numerical analysis of simultaneous heat and mass transfer during infiltration into frozen ground. *Journal of Hydrology* **200**: 345–363.